Calculation of the Vibronic Fine Structure in Electronic Spectra at Higher Temperatures. 1. Benzene and Pyrazine

R. Berger,† C. Fischer, and M. Klessinger*

Organisch-Chemisches Institut der Westfälischen Wilhelms-Universität, Corrensstrasse 40, D-48149 Münster, Germany

Received: March 24, 1998; In Final Form: June 10, 1998

A program HOTFCHT for computing the vibronic fine structure of electronic spectra at different temperatures has been developed for a theoretical investigation of the temperature dependence of absorption and fluorescence spectra of organic molecules and a discussion of the temperature dependence of their photophysical properties. The program is based on the time-independent approach using the adiabatic and harmonic approximations. A Taylor series expansion of the electronic transition dipole moment takes into account vibronic coupling similar to a first-order Herzberg−Teller treatment. For the calculation of the Franck−Condon and Herzberg−Teller integrals, the recurrence formulae of Doktorov et al. (*J. Mol. Spectrosc.* **1977**, *64*, 302) were used while the derivatives of the electronic transition dipole moment were obtained numerically. As a first application of this program the vibronic fine structure of the S_0-S_1 transitions of benzene and pyrazine were calculated at different temperatures. The equilibrium geometries and frequencies determined at the CASSCF level as well as the calculated spectra are in good agreement with experimental data; the main features of the spectra and especially "hot" bands are well-reproduced and can be assigned to the corresponding vibronic transitions.

1. Introduction

Hot bands play an important role in electronic spectra of organic molecules: they form the basis for assignment of Franck−Condon forbidden transitions like the 260 nm absorption band of benzene, and they are of particular importance in hot intermediates, as they carry the information on how these intermediates have been generated. Most importantly, thermally excited levels dominate the density of states at room temperature and therefore determine the temperature dependence of photophysical properties such as internal conversion and the rate constants of all radiative and nonradiative deactivation processes.[1] It is therefore of great theoretical and practical interest to be able to calculate spectra at higher temperatures.

The calculation of electronic spectra may be achieved either by time-dependent approaches (see, e.g., ref 2) or in terms of Franck−Condon overlaps of the initial nuclear wave functions with time-independent vibrational eigenfunctions of the final electronic state. For low resolution and very high density of states, that is, for large molecules at high temperatures, the use of time-dependent wave packets for computing spectra is particularly advantageous, while for high resolution and room temperature time-independent approaches might be preferable. Although the diabatic transition dipole moments are, in contrast to the adiabatic ones, only slowly varying functions of nuclear coordinates,[3] the adiabatic representation has the advantage of being directly applicable to the commonly computed adiabatic potential energy surfaces.

The prevalent approach to vibronic spectra calculation is the Franck−Condon (FC) approximation, which requires the evaluation of multidimensional overlap integrals of vibrational wave functions, commonly known as Franck−Condon integrals.[4] Different methods[5−11] have been proposed for an evaluation of these integrals. First applications to larger molecules were based on the QCFF/PI method of Warshel and Karplus[12] (force field combined with a quantum-chemical description of the π system) or the CNDO/S method of del Bene and Jaffé.[13] Vibronic coupling effects may be taken into account within the Herzberg−Teller (HT) approximation.[14] Similarly, a Taylor series expansion of the electronic transition dipole moment similar to an *n*th-order HT treatment[15] can be used (see, e.g., ref 16). Applications of the FC-HT treatment based on the semiempirical QCFF/PI method[17] as well as on ab initio CIS calculations[18,19] or on CASSCF calculations[16,20] have been reported; the agreement with experimental spectra is moderate to good.

Calculations of vibronic spectra at higher temperatures are scarce; one of the problems is the systematic generation of the combinations of vibrational quantum numbers for the transitions that fall into a given spectral interval. The common algorithms[21,22] are applicable only to zero vibrational quantum numbers in the initial state. We therefore extended the backtracking procedure of Kemper, van Dijk, and Buck (KDB)[22] to include vibrational excited levels in the initial state.[23] On the basis of this method and the general analysis of FC integrals by Doktorov et al.,[7] we developed the generally applicable program HOTFCHT for the calculation of vibronic spectra at higher temperatures.[24]

In this paper the program HOTFCHT will be described briefly and applied to absorption and emission spectra of benzene and pyrazine. In section 2 the derivation of the general expressions for multidimensional FC integrals including the Dushinsky effect given by Doktorov et al.[7] is reviewed, explicit formulae for the FC and HT integrals used in the program are stated, and the general structure of the program is outlined. Computational

* Corresponding author. Email: klessim@uni-muenster.de.
† Present address: Laboratorium für Physikalische Chemie, ETH Zürich (Zentrum), CH-8092 Zürich, Switzerland.

S1089-5639(98)01597-7 CCC: $15.00
Published on Web 08/18/1998

details are given in section 3, and results are presented in sections 4 and 5.

2. Theoretical Method and Its Implementation

The intensity $I_{\kappa\mu}$ of an electric dipole transition between two vibronic states $|\kappa(\vec{q}, \vec{Q})\rangle$ and $|\mu(\vec{q}, \vec{Q})\rangle$ is proportional to the square of the electric transition dipole moment $\vec{M}_{\kappa\mu}$ and to the population $W(\mu)$ of the initial vibronic state $|\mu\rangle$ as well as to the transition frequency $\tilde{\nu}_{\kappa\mu}$ or its fourth power for absorption or emission processes, respectively.[25] That is

$$I_{\kappa\mu} \sim \tilde{\nu}_{\kappa\mu} W(\mu) |\vec{M}_{\kappa\mu}|^2 \quad \text{for} \quad \text{absorption}$$

$$I_{\kappa\mu} \sim \tilde{\nu}^4_{\kappa\mu} W(\mu) |\vec{M}_{\kappa\mu}|^2 \quad \text{for} \quad \text{emission} \tag{1}$$

In the adiabatic approximation the electric transition dipole moment reads

$$\begin{aligned} \vec{M}_{\kappa\mu} &\approx \langle \chi_{k,\kappa}(\vec{Q}) | \langle \psi_k(\vec{q}, \vec{Q}) | \vec{M}(\vec{q}, \vec{Q}) | \psi_m(\vec{q}, \vec{Q}) \rangle | \chi_{m,\mu}(\vec{Q}) \rangle \\ &= \langle \chi_{k,\kappa}(\vec{Q}) | \vec{M}_{km}(\vec{Q}) | \chi_{m,\mu}(\vec{Q}) \rangle \end{aligned} \tag{2}$$

where $|\psi_k(\vec{q}, \vec{Q})\rangle$ or $|\psi_m(\vec{q}, \vec{Q})\rangle$ and $|\chi_{k,\kappa}(\vec{Q})\rangle$ or $|\chi_{m,\mu}(\vec{Q})\rangle$ denote the final (k, κ) or initial (m, μ) electronic and vibrational states, respectively, $\vec{M}_{km}(\vec{Q})$ is the electronic transition dipole moment, and $\vec{q}$ and $\vec{Q}$ represent the collected electronic or nuclear coordinates.

Owing to the parametric dependence of the electronic Born−Oppenheimer (BO) wave function on the nuclear coordinates, it is in general not possible to obtain an analytic expression for $\vec{M}_{km}(\vec{Q})$. Therefore, approximate methods are needed to treat the $\vec{Q}$ dependence of $\vec{M}_{km}$. A Taylor expansion of the electronic transition dipole moment about the equilibrium geometry $\vec{Q}_0$ of the initial electronic state yields

$$\begin{aligned} \vec{M}_{km}(\vec{Q}) \underset{\vec{Q}\to\vec{Q}_0}{\approx} \vec{M}_{km}(\vec{Q}_0) + \sum_{\eta=1}^{N} \left(\frac{\partial \vec{M}_{km}(\vec{Q})}{\partial Q_\eta} \right)_{\vec{Q}_0} (Q_\eta - Q^0_\eta) + \\ \frac{1}{2} \sum_{\eta=1}^{N} \sum_{\zeta=1}^{N} \left(\frac{\partial^2 \vec{M}_{km}(\vec{Q})}{\partial Q_\eta \partial Q_\zeta} \right)_{\vec{Q}_0} (Q_\eta - Q^0_\eta)(Q_\zeta - Q^0_\zeta) + O[(\vec{Q} - \vec{Q}_0)^3] \end{aligned} \tag{3}$$

where N is the number of vibrational degrees of freedom.

Truncation of the expansion after the constant term yields the Franck−Condon (FC) approximation,[4] which neglects the $\vec{Q}$ dependence of the electronic transition dipole moment. This approximation is quite sufficient in many cases; for the investigation of the Franck−Condon forbidden $^1A_{1g}-{}^1B_{2u}$ transition in benzene and of the weakly allowed $^1A_g-{}^1B_{3u}$ transition in pyrazine, however, higher order terms are required. Keeping first-order terms only yields

$$\begin{aligned} \vec{M}_{\kappa\mu} = \vec{M}_{km}(\vec{Q}_0) \langle \chi_{k,\kappa}(\vec{Q}) | \chi_{m,\mu}(\vec{Q}) \rangle + \\ \sum_{\eta=1}^{N} \left(\frac{\partial \vec{M}_{km}(\vec{Q})}{\partial Q_\eta} \right)_{\vec{Q}_0} \langle \chi_{k,\kappa}(\vec{Q}) | \hat{Q}_\eta - \hat{Q}^0_\eta | \chi_{m,\mu}(\vec{Q}) \rangle \end{aligned} \tag{4}$$

The derivatives of the electronic transition dipole moment with respect to the nuclear coordinates may be obtained analytically by the Herzberg−Teller (HT) expansion of the electronic wave function[14] or by numerical differentiation. The latter method, which is applied in the present work, requires careful consideration of the relative signs of the partial derivatives, as has been pointed out also for the interference of FC and HT contributions.[26]

The computer program HOTFCHT developed for the calculation of vibronic spectra including hot bands by means of the Franck−Condon or Herzberg−Teller approximation, makes use of the harmonic approximation in calculating the FC integrals $\langle \chi_{k,\kappa}(\vec{Q}) | \chi_{m,\mu}(\vec{Q}) \rangle$ and the HT integrals $\langle \chi_{k,\kappa}(\vec{Q}) | \hat{Q}_\eta | \chi_{m,\mu}(\vec{Q}) \rangle$ by assuming that the vibrational wave function of the initial and final electronic states can be described by eigenstates of the N-dimensional harmonic oscillator, i.e., by setting $|\chi_{k,\kappa}\rangle \Rightarrow |\vec{v}'\rangle$ and $|\chi_{m,\mu}\rangle \Rightarrow |\vec{v}\rangle$. The components Q_η of the vector $\vec{Q}$ are then mass-weighted normal coordinates of the initial electronic state and differ in general from the normal coordinates $\vec{Q}'$ of the final electronic state by the Dushinsky transformation[27]

$$\vec{Q}' = \mathbf{S}\vec{Q} + \vec{d} \tag{5}$$

$\mathbf{S}$ is an orthogonal $N \times N$ matrix describing a rotation in the N-dimensional normal coordinate space, and $\vec{d}$ is an N-dimensional vector specifying a translation in this space. Note that in order to calculate the matrix $\mathbf{S}$ and the vector $\vec{d}$ for a given molecule with N vibrational degrees of freedom a proper choice of the orientation of the initial and final electronic state geometries must be chosen. (For a discussion see the appendix of ref 28 and refs 10, 29.) Starting from the coherent states $|\vec{\alpha}\rangle$ of the N-dimensional harmonic oscillator, Doktorov et al.[7] derived recurrence relations for the FC integrals $\langle \vec{v}' | \vec{v} \rangle$ including the Dushinsky effect, treating the excitation process as a sudden transition and ignoring vibrational−rotational coupling effects.

According to

$$|\vec{\alpha}\rangle = e^{-(1/2)|\vec{\alpha}|^2} \sum_{v_1,\ldots,v_N=0}^{\infty} \left[\prod_{\zeta=1}^{N} \left(\frac{\alpha_\zeta^{v_\zeta}}{\sqrt{v_\zeta!}} \right) \right] |v_1, \ldots, v_N\rangle \tag{6}$$

the $|\vec{\alpha}\rangle$ serve as the generating functions for the stationary states of the initial harmonic oscillator. A coordinate space representation of the coherent states is given by

$$\begin{aligned} |\vec{\alpha}\rangle \underset{\text{coordinate space}}{\hat{=}} (\pi\hbar)^{-N/4} [\prod_{\eta=1}^{N} \omega_\eta]^{1/4} \exp\left[\sum_{\eta=1}^{N} \left(-\frac{\omega_\eta}{2\hbar} Q_\eta^2 + \right.\right. \\ \left.\left. \sqrt{\frac{2\omega_\eta}{\hbar}} \alpha_\eta Q_\eta - \frac{1}{2}\alpha_\eta^2 - \frac{1}{2}|\alpha_\eta|^2 \right) \right] \end{aligned}$$

A similar expression is readily obtained for the coherent state $|\vec{\gamma}\rangle$ of the final state harmonic oscillator by substituting Q'_η for Q_η, γ_η for α_η and ω'_η for ω_η. Expressing Q'_η through Q_η by the Dushinsky relation and utilizing the Gaussian integral $\int_{-\infty}^{\infty}\cdots\int \exp(-1/2\vec{x}^{\mathrm{T}}\mathbf{A}\vec{x} + \vec{b}^{\mathrm{T}}\vec{x})\mathrm{d}x_1\ldots\mathrm{d}x_N = (2\pi)^N(\det \mathbf{A})^{-1/2} \exp({}^1/_2\vec{b}^{\mathrm{T}}\mathbf{A}^{-1}\vec{b})$ yields the overlap integral $\langle \vec{\gamma} | \vec{\alpha} \rangle$[7]

$$\begin{aligned} \langle \vec{\gamma} | \vec{\alpha} \rangle = \langle \vec{0}' | \vec{0} \rangle \exp\left[-\frac{1}{2}(|\vec{\alpha}|^2 + |\vec{\gamma}|^2) \right] \exp\left[-\frac{1}{2}(\vec{\alpha}^{\mathrm{T}}\vec{\gamma}^{*\mathrm{T}}) \right. \\ \left. \begin{pmatrix} \mathbf{1} - 2\mathbf{Q} & -2\mathbf{R} \\ -2\mathbf{R}^{\mathrm{T}} & \mathbf{1} - 2\mathbf{P} \end{pmatrix} \begin{pmatrix} \vec{\alpha} \\ \vec{\gamma}^* \end{pmatrix} + \sqrt{2}(\vec{\alpha}^{\mathrm{T}}\vec{\gamma}^{*\mathrm{T}}) \begin{pmatrix} -\mathbf{R} & \mathbf{0} \\ \mathbf{0} & \mathbf{1} - \mathbf{P} \end{pmatrix} \begin{pmatrix} \vec{\delta} \\ \vec{\delta} \end{pmatrix} \right] \end{aligned} \tag{7}$$

Here, the symmetric positive-definite $N \times N$ matrices $\mathbf{Q}$ and $\mathbf{P}$ and the $N \times N$ matrix $\mathbf{R}$ are defined as

$$\mathbf{Q} = (1 + \mathbf{J}^{\mathrm{T}}\mathbf{J})^{-1}, \quad \mathbf{P} = \mathbf{J}\mathbf{Q}\mathbf{J}^{\mathrm{T}}, \quad \mathbf{R} = \mathbf{Q}\mathbf{J}^{\mathrm{T}}$$

where

$$\mathbf{J} = \lambda_{\omega'}\mathbf{S}\lambda_{\omega}^{-1}, \quad \lambda_{\omega} = \mathrm{diag}(\sqrt{\omega_1},...,\sqrt{\omega_N}), \quad \text{and} \quad \vec{\delta} = \hbar^{-1/2}\lambda_{\omega'}\vec{d}$$

and $\mathbf{S}$ and $\vec{d}$ specify the Dushinsky transformation eq 5.

The overlap integral $\langle 0'|0\rangle$ is given by

$$\langle \vec{0}'|\vec{0}\rangle = 2^{N/2}\left[\prod_{\eta=1}^{N}\frac{\omega_\eta}{\omega'_\eta}\right]^{1/4}\sqrt{\det \mathbf{Q}}\,\exp\left[-\frac{1}{2}\vec{\delta}^{\mathrm{T}}(\mathbf{1}-\mathbf{P})\vec{\delta}\right] \quad (8)$$

Following Sharp et al.[5] the $\langle\vec{0}'|\vec{0}\rangle$ is normalized using the additional factor $[\det \mathbf{S}]^{-1/2}$, which equals 1 for an ideal N-dimensional harmonic oscillator. According to eq 6, the overlap integrals $\langle\vec{\gamma}|\vec{\alpha}\rangle$ of the coherent states serve as the generating functions of the stationary states:

$$\langle\vec{\gamma}|\vec{\alpha}\rangle = \exp\left[-\frac{1}{2}(|\vec{\alpha}|^2+|\vec{\gamma}|^2)\right]\sum_{v_1,...,v_N,v'_1,...,v'_N=0}^{\infty}\left[\prod_{\zeta=1}^{N}\left(\frac{\alpha_\zeta^{v_\zeta}\gamma_\zeta^{*v_\zeta}}{v_\zeta!v'_\zeta!}\right)\right]\langle v'_1,...,v'_N|v_1,...,v_N\rangle \quad (9)$$

Combining eqs 7 and 9 yields

$$\langle\vec{0}'|\vec{0}\rangle\exp\left[-\frac{1}{2}(\vec{\alpha}^{\mathrm{T}}\vec{\gamma}^{*\mathrm{T}})\begin{pmatrix}\mathbf{1}-2\mathbf{Q} & -2\mathbf{R}\\ -2\mathbf{R}^{\mathrm{T}} & \mathbf{1}-2\mathbf{P}\end{pmatrix}\begin{pmatrix}\vec{\alpha}\\ \vec{\gamma}^*\end{pmatrix}+\sqrt{2}\,(\vec{\alpha}^{\mathrm{T}}\vec{\gamma}^{*\mathrm{T}})\begin{pmatrix}-\mathbf{R} & \mathbf{0}\\ \mathbf{0} & \mathbf{1}-\mathbf{P}\end{pmatrix}\begin{pmatrix}\vec{\delta}\\ \vec{\delta}\end{pmatrix}\right] = \sum_{v_1,...,v_N,v'_1,...,v'_N=0}^{N}\left[\prod_{\delta=1}^{N}\left(\frac{\alpha_\delta^{v_\delta}\,\gamma_\delta^{*v'_\delta}}{\sqrt{v_\zeta!v'_\zeta!}}\right)\right]\langle v'_1,...,v'_N|v_1,...,v_N\rangle \quad (10)$$

Starting from eq 10, Doktorov et al.[7] obtained recurrence formulae by differentiating both sides with respect to α_η, using eq 10 again to substitute the unmodified exponential by the power expansion and collecting equal powers of $\{\alpha_\zeta\}$ and $\{\gamma^*_\zeta\}$ yielding eq 11, and carrying out the same procedure for γ^*_ξ yielding eq 12:

$$\langle\vec{v}'|v_1,...,v_\eta+1,...,v_N\rangle = 2\sum_{\xi=1}^{N}R_{\eta\xi}\sqrt{\frac{v'_\xi}{v_\eta+1}}\langle v'_1,...,v'_\xi-1,...,v'_N|v_1,...,v_\eta,...,v_N\rangle + \sum_{\zeta=1}^{N}(2\mathbf{Q}-\mathbf{1})_{\eta\zeta}\sqrt{\frac{v_\zeta}{v_\eta+1}}\langle\vec{v}|v_1,...,v_\zeta-1,...,v_N\rangle - \sqrt{\frac{2}{v_\eta+1}}(\mathbf{R}\vec{\delta})_\eta\langle\vec{v}'|v_1,...,v_\eta,...,v_N\rangle \quad (11)$$

$$\langle v'_1,...,v'_\xi+1,...,v'_N|\vec{v}\rangle = 2\sum_{\eta=1}^{N}R_{\xi\eta}\sqrt{\frac{v_\eta}{v'_\xi+1}}\langle v'_1,...,v'_\xi,...,v'_N|v_1,...,v_\eta-1,...,v_N\rangle + \sum_{\vartheta=1}^{N}(2\mathbf{P}-\mathbf{1})_{\xi\vartheta}\sqrt{\frac{v'_\vartheta}{v'_\xi+1}}\langle v'_1,...,v'_\vartheta-1,...,v'_N|\vec{v}\rangle + \sqrt{\frac{2}{v'_\xi+1}}[(\mathbf{1}-\mathbf{P})\vec{\delta}]_\xi\langle v'_1,...,v'_\xi,...,v'_N|\vec{v}\rangle \quad (12)$$

By means of these recurrence relations, all necessary FC integrals of a molecule with N vibrational degrees of freedom may be calculated; these relations thus permit a calculation of the vibrational fine structure of electronic transitions in the FC approximation.

In order to include HT terms as well, the algebraic properties of the ladder operators of the N-dimensional harmonic oscillator are used to express the HT integrals as a sum of FC integrals, yielding

$$\langle\vec{v}'|\hat{Q}_\eta|\vec{v}\rangle = \sqrt{\frac{\hbar}{2\omega_\eta}}[\sqrt{v_\eta}\langle\vec{v}'|v_1,...,v_\eta-1,...,v_N\rangle + \sqrt{v_\eta+1}\langle\vec{v}'|v_1,...,v_\eta+1,...,v_N\rangle] \quad (13)$$

Similarly, all integrals of the general type $\langle\vec{v}'|\hat{Q}_1^{k_1}\hat{Q}_2^{k_2}...\hat{Q}_N^{k_N}|\vec{v}\rangle$ and $\langle\vec{v}'|\hat{P}_1^{k_1}\hat{P}_2^{k_2}...\hat{P}_N^{k_N}|\vec{v}\rangle$ with $k_\eta \in \mathrm{N}_0$ may be expanded in terms of FC integrals.

In order to allow for anharmonicity effects, the potential energy $V(\vec{Q})$ is expanded in terms of one-dimensional functions of the general type $y^k\exp(\alpha y)$, where $y = [(m\omega_e)/\hbar]^{-1/2}Q_\eta$, $k \in \mathrm{N}_0$, and $\eta = 1, ..., N$.

Using the properties of the ladder operators, Duch[30] derived the following analytic formulae for matrix elements of the one-dimensional harmonic oscillators

$$\langle v_\eta|y^k|w_\eta\rangle = 2^{j-k/2}\left(\frac{w_\eta!}{v_\eta!}\right)^{1/2}k!\sum_i\frac{v_\eta!}{2^i i!(v_\eta-i)!(w_\eta-i)!(i-j)!} \quad (14)$$

where $j = {}^1/_2(v_\eta + w_\eta - k)$ and $\max(0, j) \le i \le \min(v_\eta, w_\eta)$, and

$$\langle v_\eta|y^k\exp(\alpha y)|w_\eta\rangle\exp(\alpha^2/4)\left(\frac{\alpha}{\sqrt{2}}\right)^{-w_\eta}\times\sqrt{w_\eta!}\sum_{j=0}^{w_\eta}\sum_{l=w_\eta-j}^{v_\eta+k}{}'\frac{(\alpha/\sqrt{2})^{2j+l}\sqrt{l!}}{j!(w_\eta-j)!(j+l-w_\eta)!}\langle v_\eta|y^k|l\rangle \quad (15)$$

where the primed summation is performed only if $(w_\eta - j) \le (v_\eta + k)$.

These expressions can be used in a variational procedure to expand the bound eigenstates of one-dimensional anharmonic oscillators in terms of harmonic oscillator states. This procedure is employed to obtain the FC and HT integrals of double well potentials by means of the recurrence relations eqs 11 and 12. A proper treatment of anharmonicity, however, would require the computation of an N-dimensional anharmonic potential energy surface and the diagonalization of the resulting Hamiltonian matrix to yield the eigenstates and eigenvalues of the N-dimensional anharmonic oscillator. Since all cross-terms between Q_η and Q_ζ with $\eta \neq \zeta$ are ignored in our anharmonic potential energy surface $V(\vec{Q})$ as well as angular momentum terms in the kinetic energy, the Hamiltonian is still separable in the normal coordinates, but only a crude estimate of anharmonic effects is expected.

Finally, in order to include hot bands in the spectral calculation, the population probability $W(\mu)$ of the initial vibronic state has to be taken into account explicitly. In the harmonic approximation used here, $W(\mu)$ becomes $W(\vec{v})$, and assuming a Boltzmann distribution for a system in thermal equilibrium one obtains[31]

$$W(\vec{v}, T) = W(\vec{0}, T) \exp\left[-\frac{\hbar\sum_{\eta=1}^{N} v_\eta \omega_\eta}{kT}\right] \qquad (16)$$

where

$$W(\vec{0}, T) = \prod_{\eta=1}^{N}\left[1 - \exp\left(-\frac{\hbar\omega_\eta}{kT}\right)\right]$$

In order to calculate the temperature-dependent spectra with the program HOTFCHT, the following input data are required, which can be obtained from the usual quantum chemistry programs at various levels of sophistication:

1. Equilibrium geometries of the molecule in the electronic states under consideration.

2. Normal coordinates in mass-weighted Cartesian displacement coordinates and harmonic frequencies of the electronic states of interest.

3. The electronic transition dipole moment at the equilibrium geometry of the initial electronic state and its derivatives with respect to the normal coordinates.

4. If anharmonic effects are to be included, a cut through the potential energy surface along selected normal coordinates fitted to a function of the general type $f(Q_\eta) = \sum_k c_k([(m\omega)/\hbar]^{1/2}Q_\eta)^k \exp[\alpha_k[(m\omega)/\hbar]^{1/2}Q_\eta]$.

Using these input data, the **S** matrix and the vector $\vec{\delta}$ are determined first; next the matrices **J**, **Q**, **R**, and **P** are evaluated and $\langle\vec{0}'|\vec{0}\rangle$ is computed. Finally $2\mathbf{R}$, $(2\mathbf{Q} - \mathbf{1})$, $(2\mathbf{P} - \mathbf{1})$, $\sqrt{2}\mathbf{R}\vec{\delta}$, and $\sqrt{2}(\mathbf{1} - \mathbf{P})\vec{\delta}$ are evaluated and stored for further calculation.

After the spectrum is divided into intervals according to the desired resolution, all transition energy levels (that is, all combinations of quantum numbers of the initial and final state specifying a certain transition) connected with a sufficiently populated initial vibronic state are generated by the backtracking procedure described elsewhere.[23] As all combination bands and overtones are generated in this procedure, a large number of transitions is obtained. For each of these transitions, the electronic transition dipole moment is calculated according to eq 4 using the FC and HT integrals obtained from the recurrence formulae. Owing to the large number of transitions, the integrals are not kept in core as suggested in ref 32 but calculated directly as described in the Appendix.

If anharmonic effects are to be included, overlap integrals of the general type

$$\sum_{\substack{v_1,\ldots,v_N,\\ v_1',\ldots,v_{N=0}'}}^{\infty} \left(\prod_{\eta=4}^{N} c_{v_\eta'} c_{v_\eta}\right)\langle v_1', \ldots, v_N'|v_1, \ldots, v_N\rangle$$

have to be evaluated for each transition, where the c_{v_η} and $c_{v_\eta'}$ are the expansion coefficients of the one-dimensional anharmonic oscillator states in the basis of one-dimensional harmonic oscillator states. Note that couplings between several normal modes can be included via expanding the vibrational states in the basis of the *N*-dimensional oscillator states; this is, however, currently not yet implemented in the program.

3. Computational Details

Ground- and excited-state geometries were optimized on the CASSCF level using a double-ζ basis set[33] augmented by a set of polarization functions (DZP) for benzene and a valence double-ζ basis set[33] augmented by a set of polarization functions (DZVP) for pyrazine. The active space was chosen to contain the six π and π^* MOs and, in the case of pyrazine, the two nitrogen lone-pair orbitals. Harmonic frequencies and normal coordinates were calculated at the optimized geometries using analytic derivatives of the energy with respect to nuclear coordinates. The GAUSSIAN 94 package[34] was used for the geometry optimization of pyrazine and the vibrational analyses, while the geometries of benzene were optimized with the GAMESS program.[35]

The first derivatives of the electronic transition dipole moment with respect to the normal coordinates were determined numerically, the displacements being $0.02\sqrt{u}$ Å (benzene) or $0.01\sqrt{u}$ Å (pyrazine). Single-point calculations at these nonequilibrium geometries were performed with the GAMESS program using the state-averaged method. This method shows a good convergence and yields a common set of MOs for S_0 and S_1, thus simplifying considerably the determination of transition dipole moments.

The MRCI energy profile of the pyrazine mode ν_{10a} was calculated with the progam system MOLPRO 96,[36] which makes use of the internally contracted MRCI method.[37]

The HOTFCHT program described in the previous section was used to determine the spectra, using an interval width of 10 cm^{-1} and a half-width of 20 cm^{-1} in plotting the spectra.

4. Benzene: Results and Discussion

The S_0 ($^1A_{1g}$) − S_1 ($^1B_{2u}$) transition of benzene has been studied in great detail experimentally as well as theoretically[31,38−47] and has been used by many authors as a test case for vibronic spectra calculation.[7,8,11,18] The reason is the relatively small number of lines due to the high symmetry of both electronic states as well as the fact that this transition is Franck−Condon forbidden and thus particularly suited for studying vibronic coupling effects. Some details of the spectra can be described quite well by simple models with few empirical parameters,[40,43,46,48] and numerous harmonic force fields based on experimental or theoretical data have been proposed that can reproduce the spectra with an accuracy of a few cm^{-1}.[18,49,50] These force fields, however, are mostly not general enough to be transferred without modifications to other molecules or electronic states, although it has been shown for benzene and naphthalene that scaling factors of the ground-state force field may also apply to the lowest excited covalent singlet state.[50]

We also use the benzene S_0-S_1 transition to test our method to calculate spectra at higher temperatures. The hot bands in addition to the above mentioned features make this transition particularly suited for such studies. Such calculations of vibronic spectra represent a severe test of the calculated frequencies and normal coordinates, that is, of the detailed shapes of the potential energy surfaces involved in these transitions. The final aim of the calculation of vibrational spectra at higher temperatures is to assist experimentalists in identifying hot intermediates and in assigning spectral lines, as well as to establish a complete description of photophysical properties including temperature effects. As in these kinds of application an adjustment of the force field to reproduce experimental data is usually not possible, we did not scale the calculated frequencies in our calculations of the benzene spectra.

CASSCF Results. Equilibrium geometries of the ground state ($^1A_{1g}$) and the first excited singlet state ($^1B_{2u}$), which both exhibit the full D_{6h} symmetry, are given in Table 1. The maximum deviation between calculated and experimental bond lengths is 0.007 Å, with the calculated CC bond distance being larger and the CH distance shorter than the experimental values.

TABLE 1: Equilibium Geometries (Å) of the $^1A_{1g}$ (S_0) and $^1B_{2u}$ (S_1) States of Benzene

	$^1A_{1g}$		$^1B_{2u}$	
parameter	CASSCF DZP[a]	exptl[b]	CASSCF DZP[c]	exptl[b]
r(CC)	1.401	1.397	1.439	1.432
r(CH)	1.076	1.079	1.074	1.075

[a] $-230.803\,47E_h$. [b] Reference 79. [c] $-230.629\,98E_h$.

TABLE 2: Vibrational Frequencies (cm^{-1}) of the $^1A_{1g}$ and $^1B_{2u}$ States of Benzene

vibration		$^1A_{1g}$		$^1B_{2u}$	
Nummer	Irrep[a]	CASSCF DZP	exptl[b]	CASSCF DZP	exptl[b]
ν_1	a_{1g}	1033	993	963	923
ν_2	a_{1g}	3399	3074	3418	3093
ν_3	a_{2g}	1482	1350	1458	1327
ν_4	b_{2g}	713	707	482	365
ν_5	b_{2g}	1022	990	693	745
ν_6	e_{2g}	646	608	575	521
ν_9	e_{2g}	1263	1178	1237	1148
ν_8	e_{2g}	1730	1600	1665	1516
ν_7	e_{2g}	3369	3057	3389	3077
ν_{10}	e_{1g}	870	847	593	581
ν_{11}	a_{2u}	705	674	523	515
ν_{12}	b_{1u}	1086	1010	1056	
ν_{13}	b_{1u}	3358	(3057)	3381	
ν_{15}	b_{2u}	1169	1149	1254	1150
ν_{14}	b_{2u}	1333	1310	1855	1570
ν_{16}	e_{2u}	427	399	292	238
ν_{17}	e_{2u}	991	967	674	717
ν_{18}	e_{1u}	1105	1038	961	920
ν_{19}	e_{1u}	1612	1484	1533	1405
ν_{20}	e_{1u}	3388	3065	3404	3084

[a] Irreducible representation. [b] Reference 45.

This matches the CASSCF results of Swiderek et al.,[50] who owing to a smaller basis set (DZV) got slightly larger deviations from experimental values. The lengthening of the CC bond on excitation, however, is calculated to be 0.003 Å larger than experimentally observed. We therefore expect the progression of the breathing mode ν_1 of benzene to be somewhat too long in the calculated absorption and emission spectra.

Calculated harmonic frequencies at the equilibrium geometries of the ground and excited state are collected in Table 2. For the $^1A_{1g}$ state the agreement with experimental values is in the usual range with deviations between 1% and 10%. For the $^1B_{2u}$ state, however, the differences are slightly larger, particularly for the out-of-plane b_{2g} modes. The same behavior has been observed in earlier CIS[18] and CASSCF[50] studies. While the excitation of an electron from a π to a π^* MO in general leads to a decrease of the frequencies of the S_1, the Kekulé mode $\nu_{14}(b_{2u})$ undergoes a frequency exaltation in the excited state, which has been explained on the basis of a valence bond picture.[51] The calculation succeeds in reproducing this behavior qualitatively, although the calculated frequency increase $\delta\nu_{14} = 522\ cm^{-1}$ is twice as large as the experimental one ($260\ cm^{-1}$) and the CH rocking mode $\nu_{15}(b_{2u})$ is also calculated to increase by $\delta\nu_{15} = 85\ cm^{-1}$. These discrepancies are not surprising in view of the calculations of Wiberg et al.,[52] which showed that even in the ground state the correct description of the benzene b_{2u} modes is a difficult task for HF, MP2, and CISD methods. In the ground state both of these modes mix owing to their near degeneracy giving in-phase and out-of-phase combination modes. As a consequence, significant off-diagonal elements occur for these vibrations in the Dushinsky matrix.

TABLE 3: Calculated and Experimental Relative Intensities of the e_{2g} Modes in the Absorption Spectrum of Benzene

line	CASSCF DZP	exptl[a]	CIS 6-31G[b]
6_0^1	100.0	100.0	100.0
7_0^1	5.4	3.6	6.1
8_0^1	3.3	0.6	1.8
9_0^1	2.9	1.8	0.04

[a] Reference 80. [b] Reference 18.

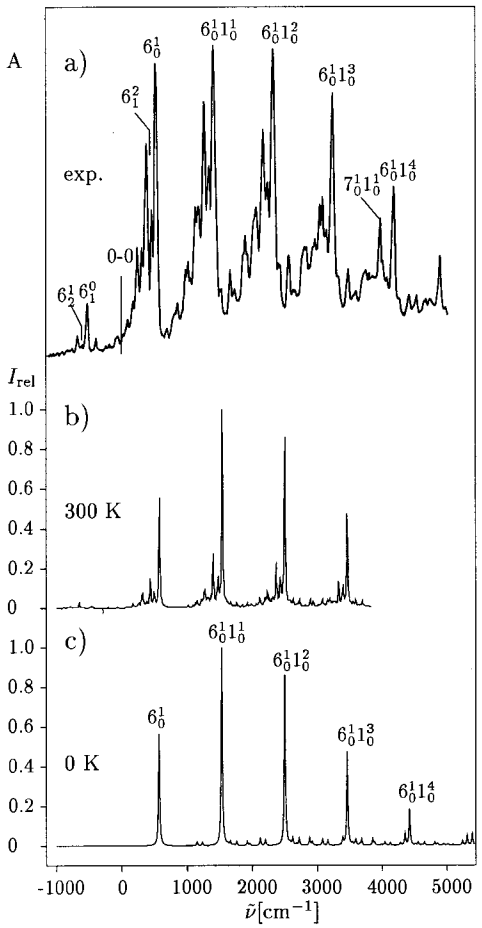

Figure 1. $^1A_{1g}-^1B_{2u}$ absorption spectrum of benzene: (a) experimental (ref 39), (b) calculated at 300 K, and (c) calculated at 0 K.

Owing to symmetry, the transition dipole moment between the $^1A_{1g}$ and $^1B_{2u}$ states vanishes. The four e_{2g} modes, however, can borrow intensity by vibronic coupling and contribute in first order to the spectra. In Table 3 the calculated relative intensities of these vibrations are compared to the experimental data. By far the most intense one is ν_6; therefore, progressions built up on this "false" origin will dominate the spectra. Compared to the experimental data, the contribution of ν_8 is slightly overestimated in our calculations.

Calculated Spectra. In Figure 1 the S_0-S_1 absorption spectrum of benzene calculated at 0 K and at 300 K is displayed together with the experimental spectrum, which shows the absorbance rather than the relative intensities according to eq 1, which are plotted for the calculated spectra. The 0 K spectrum is dominated by progressions of the totally symmetric breathing mode ν_1 with several vibronic origins. Since ν_6 is the most effective vibronic coupling mode, the main feature of the spectrum is the progression $6_0^1\,1_0^n$. While in the experimental spectrum the line 6_0^1 is more intense than $6_0^1\,1_0^2$, the calculated intensities show the reversed order. Furthermore, the calculated intensity of the line $6_0^1\,1_0^4$ is twice as high as that

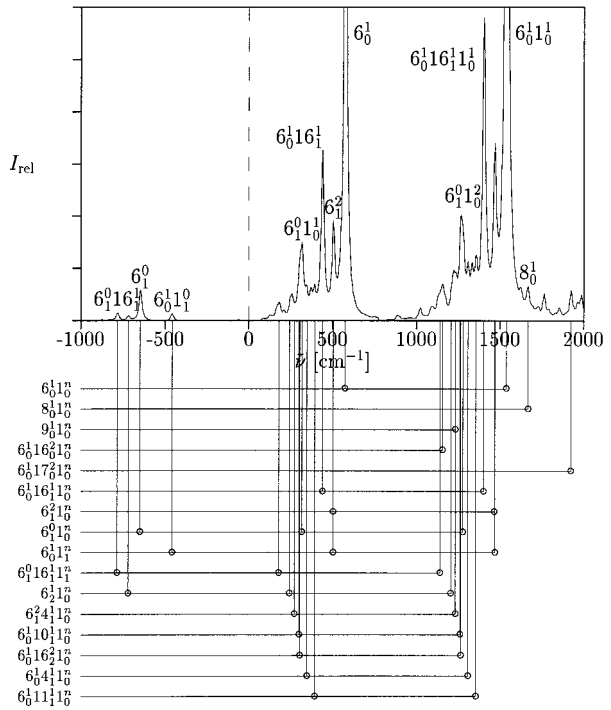

Figure 2. $^1A_{1g}-{}^1B_{2u}$ absorption spectrum of benzene calculated at 300 K.

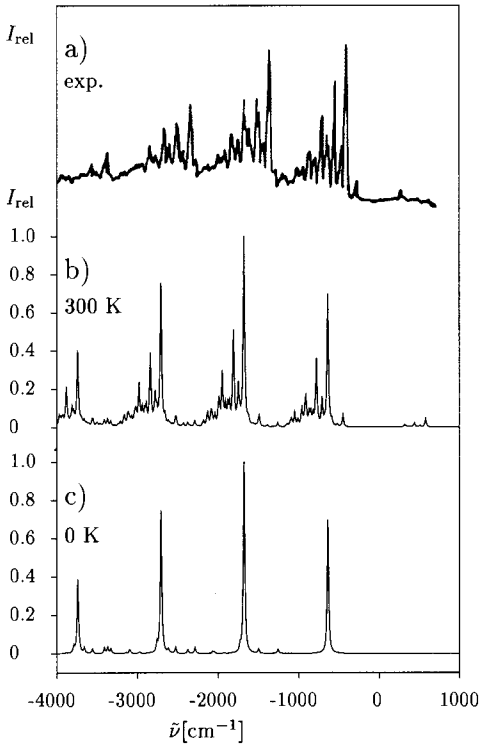

Figure 3. $^1B_{2u}-{}^1A_{1g}$ fluorescence spectrum of benzene: (a) experimental (ref 15), (b) calculated at 300 K, and (c) calculated at 0 K.

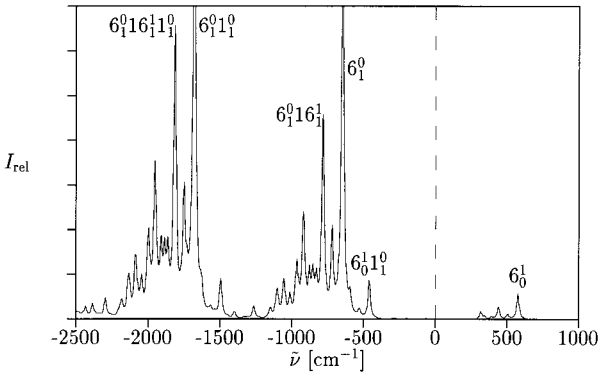

Figure 4. $^1B_{2u}-{}^1A_{1g}$ fluorescence spectrum of benzene calculated at 300 K.

of $7_0^1\,1_0^1$, while experimentally $6_0^1\,1_0^4$ is only slightly more intense than $7_0^1\,1_0^1$. These discrepancies are due to the overestimated increase of the CC bond distance on excitation, which leads to too long a progression of the breathing mode ν_1. Test calculations show that this systematic error could be easily remedied by adjusting the excited-state CC bond length. The progressions $8_0^1\,1_0^n$, $9_0^1\,1_0^n$ as well as $6_0^1\,16_0^2\,1_0^n$, $6_0^1\,17_0^2\,1_0^n$, $6_0^1\,4_0^2\,1_0^n$, $6_0^1\,5_0^2\,1_0^n$, $6_0^1\,10_0^2\,1_0^n$, and $6_0^1\,15_0^2\,1_0^n$ are significantly weaker than the progression $6_0^1\,1_0^n$, and the highest intensity is always calculated for the line with $n = 1$. Experimental fluorescence excitation spectra of jet-cooled benzene[44] show in addition some lines of comparable intensity, which are due to a second-order Herzberg−Teller effect and therefore cannot be reproduced by our first-order treatment.

At higher temperatures most of the weak lines are hidden by more intense hot bands as can be seen from Figure 1b and Figure 2, which displays in more detail a smaller fraction of the spectrum calculated at 300 K and compares quite well with the experimental spectrum shown of Figure 1a. In particular, this is true also for that part of the spectrum that shows hot bands only; the most intense absorption at longer wavelength than the 0−0 transition is the 6_1^0 line, which confirms the long known assignment of the experimental spectrum based on the assumption that this hot band involves the excited-state frequency of the mode that represents the vibronic origin of the main progression. The intensity distribution in the neighborhood of the $6_0^1\,1_0^n$ lines due to the progressions $6_0^1\,1_0^{n+1}$, $6_0^1\,16_1^1\,1_0^n$, and $6_1^2\,1_0^n$ is equally well reproduced. Figure 2 shows quite clearly that hot bands play a very significant role in room temperature spectra and that the HOTFCHT program is very well suited to reproduce these features.

The same applies to the S_1-S_0 fluorescence spectra calculated at different temperatures, which are shown in Figure 3. The dominating progressions again arise from the breathing mode ν_1 with several vibronic origins, with the progressions again being somewhat too long. At higher temperatures a rich hot-band structure shows up. The calculated spectrum in Figure 4 is in very good agreement with the experimental one displayed in Figure 3a.

5. Pyrazine: Results and Discussion

The absorption and fluorescence spectra of pyrazine have been the subject of many experimental and theoretical investigations. Owing to the D_{2h} symmetry of the molecule in the ground state S_0 ($^1A_{1g}$) as well as in the $n-\pi^*$-excited state S_1 ($^1B_{3u}$), these spectra exhibit a well-resolved vibrational fine structure, which allows the measurement of high-resolution gas-phase[53−55] and crystal spectra[56] as well as single vibronic level (SVL) spectra[53,54] and two-photon spectra.[57] In addition to Franck−Condon allowed transitions, there are lines whose intensity is due to vibronic coupling between S_1 ($^1B_{3u}$) and S_2 ($^1B_{2u}$). This interaction has been studied in detail by resonance Raman spectroscopy[58] and determination of fluorescence quantum yields.[59] Theoretical studies of the vibrational fine structure and the S_2-S_1 conical intersection have been carried out on a semiempirical[60−62] as well as on the ab initio level.[3,63] In this section we present the first calculation of the vibrational fine structure of the S_0-S_1 absorption and fluorescence band of pyrazine that takes into account on an ab initio level of theory

TABLE 4: Equilibrium Geometries (Å, deg) of the ^1A_g (S_0) and $^1B_{3u}$ (S_1) States of Pyrazine

	^1A_g			$^1B_{3u}$
parameter	CASSCF DZVP[a]	exptl[b]	exptl[c]	CASSCF DZVP[d]
r(CN)	1.333	1.13376(13)	1.339(2)	1.357
r(CC)	1.400	1.3968(30)	1.403(4)	1.387
r(CH)	1.076	1.0813(21)	1.115(4)	1.073
∠CNC	115.9	115.65(24)	115.6(4)	119.3
∠CCN	122.0	122.18(12)	122.2(4)	120.3
∠HCN	117.2	117.87(20)	113.9(10)	119.4

[a] −262.807 94E_h. [b] Reference 65. [c] Reference 66. [d] −262.633 68E_h.

TABLE 5: Vibrational Frequencies (cm^{-1}) of the ^1A_g and $^1B_{3u}$ States of Pyrazine

vibration		^1A_g		$^1B_{3u}$	
Notation[a]	Irrep[b]	CASSCF DZVP	exptl[c]	CASSCF DZVP	exptl[d]
ν_{6a}	a_g	640	596	633	585
ν_1	a_g	1076	1015	1031	970
ν_{8a}[e]	a_g	1330	1582	1265	1377
ν_{9a}[e]	a_g	1745	1230	1618	1104
ν_2	a_g	3409	3055	3437	
ν_{12}	b_{1u}	1112	1021	1417	
ν_{19a}[e]	b_{1u}	1229	1416	1026	
ν_{18a}[e]	b_{1u}	1635	1139	1588	
ν_{13}	b_{1u}	3385	3012	3422	
ν_{15}	b_{2u}	1070	1063	1468	
ν_{14}	b_{2u}	1152	1149	1382	
ν_{19b}	b_{2u}	1539	1416	1141[f]	
ν_{20b}	b_{2u}	3404	3036	3436	
ν_{6b}	b_{3g}	754	704	676	662
ν_3	b_{3g}	1473	1346	1424	
ν_{8b}	b_{3g}	1680	1525	902	
ν_{7b}	b_{3g}	3384	3040	3410	
ν_{16a}	a_u	406	341	440	400
ν_{17a}	a_u	995	960	856	743
ν_{10a}	b_{1g}	954	919	312[g]	383
ν_4[e]	b_{2g}	775	983	536	552
ν_5[e]	b_{2g}	988	756	853[f]	518
ν_{16b}	b_{3u}	456	420	250	236
ν_{11}	b_{3u}	829	785	710	

[a] Reference 67. [b] Irreducible representation. [c] Reference 68. [d] Reference 54. [e] Assignment different from ref 68 and ref 54. [f] Differing types of vibrations in ground and excited state. [g] Calculated considering the anharmonic potential.

all vibrational degrees of freedom. This is of particular importance for the determination of hot bands in the spectra calculated at higher temperatures.

CASSCF Results. Equilibrium geometries of the ground state and the first excited state of pyrazine are collected in Table 4. In agreement with recent DFT studies,[64] it may be concluded that the more recent ground-state structure derived from a combination of electron diffraction, liquid-crystal NMR, and microwave data[65] is more reliable than the older one based only on electron diffraction experiments.[66] This is particularly true for the CH distance and the HCN angle. The largest deviations between experimental and calculated data are 0.005 Å for bond distances and 0.7° for bond angles.

From the calculated structure of the S_1 ($^1B_{3u}$) state, it is seen that $n-\pi^*$ excitation leads to a more pronounced equalization of bond lengths within the ring and an appreciable increase of the CNC angles. This becomes apparent in a long progression of the ring-deformation mode ν_{6a}, which predominates the Franck−Condon contribution to the vibrational structure of the fluorescence and absorption spectra.

Calculated harmonic frequencies for the ground and excited state of pyrazine are given in Table 5. Difficulties arise in comparing these values with experimental or other theoretical

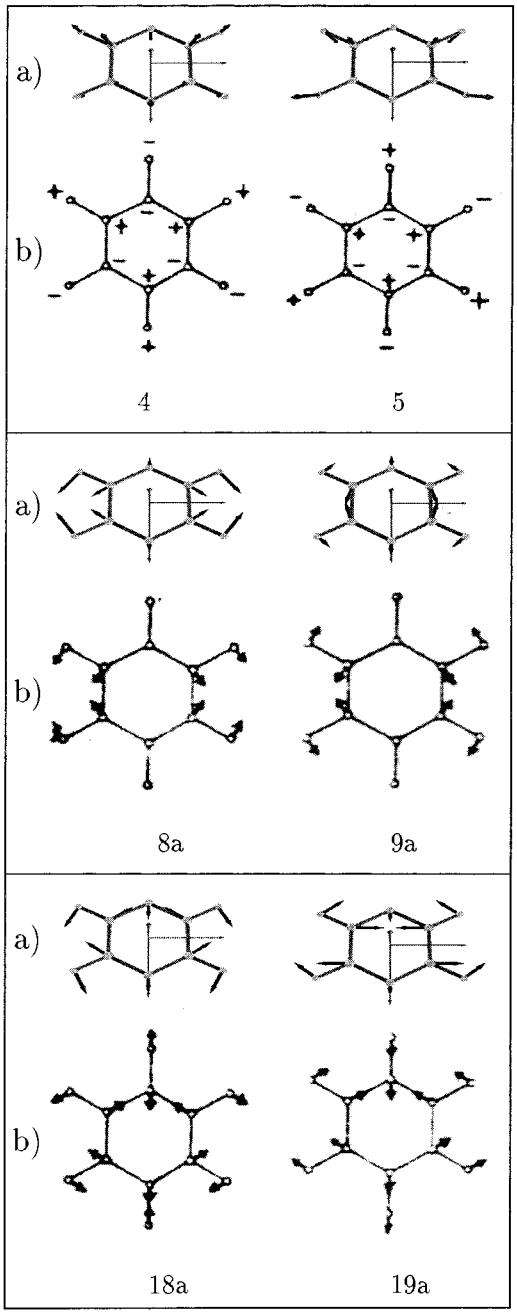

Figure 5. (a) Calculated normal coordinates compared to (b) the schematic diagrams of Lord et al.[67]

data owing to different numbering schemes of the normal modes. Lord et al.[67] proposed a scheme that follows Wilsons numbering of the benzene normal modes; replacement of CH groups by nitrogen atoms, however, not only reduces the number of vibrational degrees of freedom but also changes the form of the normal modes, which makes it hard to assign the calculated frequencies to the idealized normal modes of Lord et al. Nevertheless, the vibrational analysis for the ground state essentially confirms the assignment of Innes et al.[68] Discrepancies in nomenclature arise for the pairs ν_{8a}/ν_{9a}, ν_{18a}/ν_{19a}, and ν_4/ν_5. From Figure 5 it is seen that the normal coordinates of the members of these pairs differ only in the relative motion of carbon and hydrogen atoms. While Innes et al. assign the modes with carbon and hydrogen moving in opposite phase to the lower frequency, the calculated results correspond to the reverse assignment. Kearly et al.[69] determined atomic displacements by inelastic neutron scattering (INS); using a force field fitted

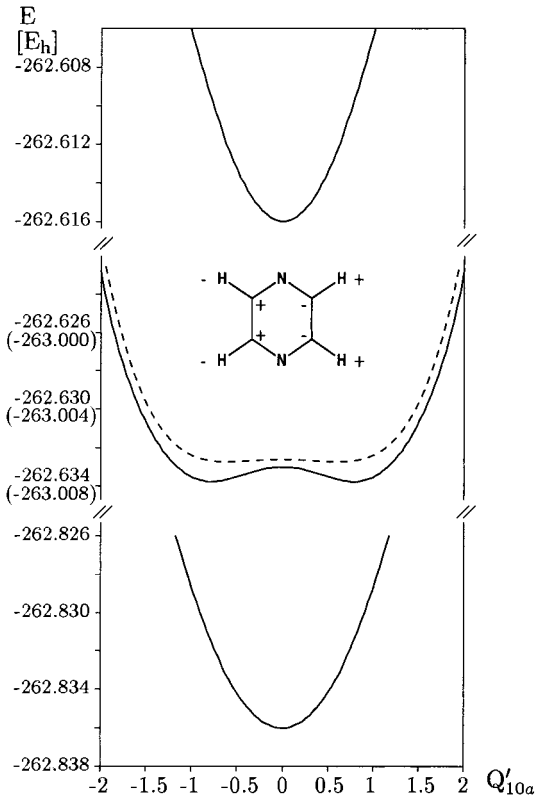

Figure 6. Calculated potential energies of S_0, S_1, and S_2 as a function of the normal coordinate 10a of the S_1 state of pyrazine.

to the INS intensities yielded an interchange of the b_{2g} vibrations ν_4 and ν_5 as compared to ab initio results. A similar behavior of ν_{8a}/ν_{9a} (a_g) as well as ν_{18a}/ν_{19a} (b_{1u}) is thus not unlikely. On the basis of these modified assignments the agreement of the calculated ground-state frequencies with experimental values is quite satisfactory; deviations are in general smaller than 10% and for frequencies above 3000 cm^{-1} smaller than 13%. Exceptions are ν_{18a} and ν_{16a}. The excited-state frequencies show a similarly good agreement with the available experimental values. A noticeable discrepancy is observed only for ν_5.

The two lowest excited states of pyrazine represent a classical example of vibronic coupling in aromatic systems.[70] From group theory it follows that first-order coupling is possible only by b_{1g} vibrations. As ν_{10a} is the only vibrational mode of this symmetry, it is possible to approximately describe the S_1-S_2 interaction by a single vibronic coupling mode.[56,71−74] If in addition totally symmetric tuning modes are included in the model, multimode effects in the spectrum can be described[75] and a S_1-S_2 conical intersection can be characterized.[3,60,63,75,76]

Owing to this vibronic coupling, the S_1 potential of the mode ν_{10a} is strongly anharmonic. From the absorption spectrum one has ν^n_{10a} = 383, 823, and 1307 cm^{-1}. Model calculations based on the absorption spectrum yield a flat energy profile,[56,72] while resonance Raman intensities suggest the occurrence of a double-minimum potential.[73] Energy profiles along the S_1 normal coordinate of ν_{10a} calculated on the CASSCF level for S_0, S_1, and S_2 are shown in Figure 6. Owing to the mutual interaction the S_2 potential is fairly steep, while the S_1 potential has a double minimum with a barrier of 295 cm^{-1}. However, if in addition dynamic correlation is taken into account, a somewhat different S_1 energy profile results. MRCI surfaces of Domcke et al.,[3] for instance, exhibit no double minimum. In order to obtain the energy profile of the ν_{10a} mode at the minimum geometry of the excited state, geometry optimizations

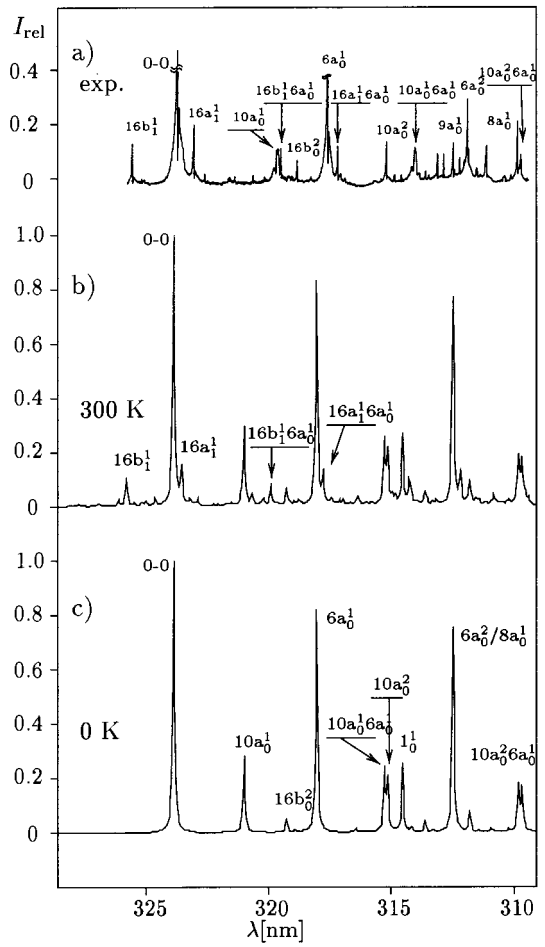

Figure 7. $^1A_g-{}^1B_{3u}$ absorption spectrum of pyrazine: (a) experimental (ref 54), (b) calculated at 300 K, and (c) calculated at 0 K.

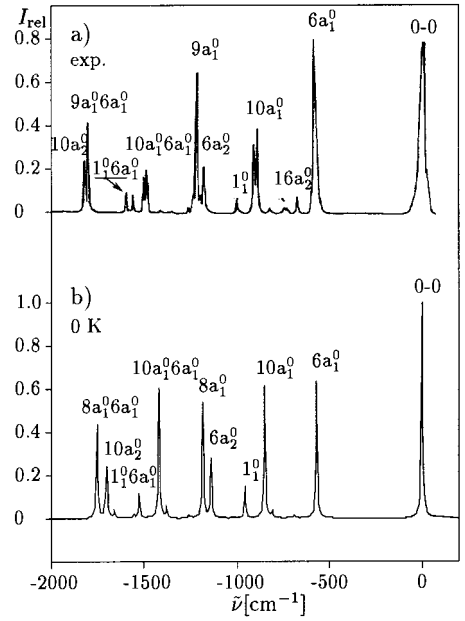

Figure 8. $^1B_{3u}-{}^1A_g$ fluorescence spectrum of pyrazine: (a) experimental (ref 53) and (b) calculated at 0 K.

restricting the symmetry to D_{2h} were carried out at the MRCI level. As it is not possible for technical reasons to include all single and double excitations with respect to the CASSCF reference, the optimization as well as the determination of the energy profile was performed keeping frozen the 11 lowest MOs, which are separated from the other MOs by a significant

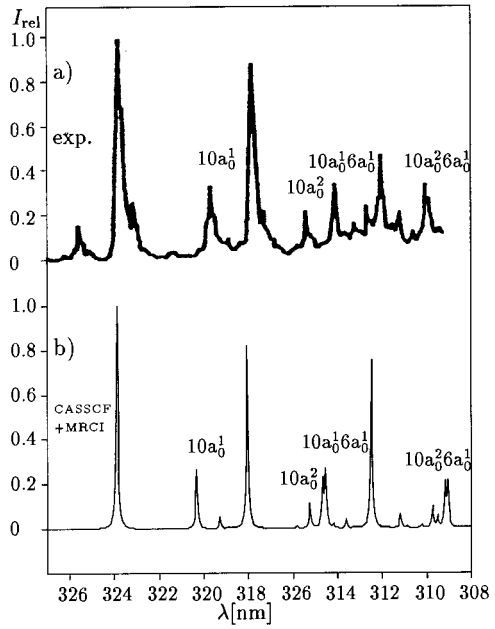

Figure 9. $^1A_g - ^1B_{3u}$ absorption spectrum of pyrazine: (a) experimental (ref 81) and (b) calculated at 0 K using the MRCI potential of the 10a mode.

energy gap. This is the smallest frozen core of ref 3. The resulting energy profile is shown in Figure 6 by a broken line and corresponds to a double minimum with a barrier of only 46 cm^{-1}. Thus, a double-minimum potential cannot be excluded, although the zero-point vibration lies already above the barrier. In order to take into account the anharmonicity of ν_{10a} in calculating the spectra, a polynomial of degree 12 was fitted to this potential, and an expansion in terms of harmonic oscillators was used to describe the vibration. This is only a crude approximation, which cannot describe the coupling with other vibrations that may arise through the anharmonicity and its effect on the vibrational structure.

Calculated Spectra. Absorption spectra of pyrazine calculated at 0 and 300 K, the fluorescence spectrum calculated at 0 K, and the absorption spectrum calculated using the MRCI potential of the mode ν_{10a} are shown together with experimental spectra in Figures 7−9, respectively. To facilate the comparison with the experimental spectra, the frequencies of the calculated spectra have been scaled by 0.9, which is a crude factor but sufficient for this application, since the scale factors for most popular basis sets are close to this value.[77] The mode ν_{6a} gives rise to the most intense progression in the absorption as well as in the fluorescence spectrum. From the good agreement between the calculated and the experimental values for the relative intensities of the totally symmetric vibrations collected in Table 6, it may be concluded that the structural changes on excitation are correctly described by the computed equilibrium geometries. The relative intensity of ν_{8a} (ν_{9a} according to Innes et al.[68]), however, differs from the experimental values in the same way as in other quantum chemical calculations of the spectra.[3,61,63] Using a force field scaled to reproduce the atomic displacements might improve the intensities. The low intensity of the ν_1 mode in the experimental spectrum has been explained by Heider and Fischer[75] by an anharmonic coupling with the first harmonic of ν_{10a}. In the experimental fluorescence spectrum the intense $10a_1^0$ line is split into *P* and *R* branches; in low-resolution spectra[71,78] where the rotational fine structure is not resolved the intensity is intermediate between those of the lines $6a_1^0$ and $8a_1^0$, in good agreement with our calculations. The correct line position, however, is reproduced only if the MRCI potential is used (Figure 9). The calculated intensities of the b_{2g} modes ν_4 and ν_5, which can borrow some intensity

TABLE 6: Calculated and Experimental Relative Intensities of the Totally Symmetric Modes in the Absorption and Fluorescence Spectrum of Pyrazine

absorption			fluorescence		
Band	CASSCF DZVP	exptl[a]	Band	CASSCF DZVP	exptl[a]
$6a_0^1$	80	80	$6a_1^0$	71	80
$6a_0^2$	32	33	$6a_2^0$	25	25
$8a_0^1$	40	18	$8a_1^0$	50	70
1_0^1	24	3	1_1^0	13	7

[a] Reference 54.

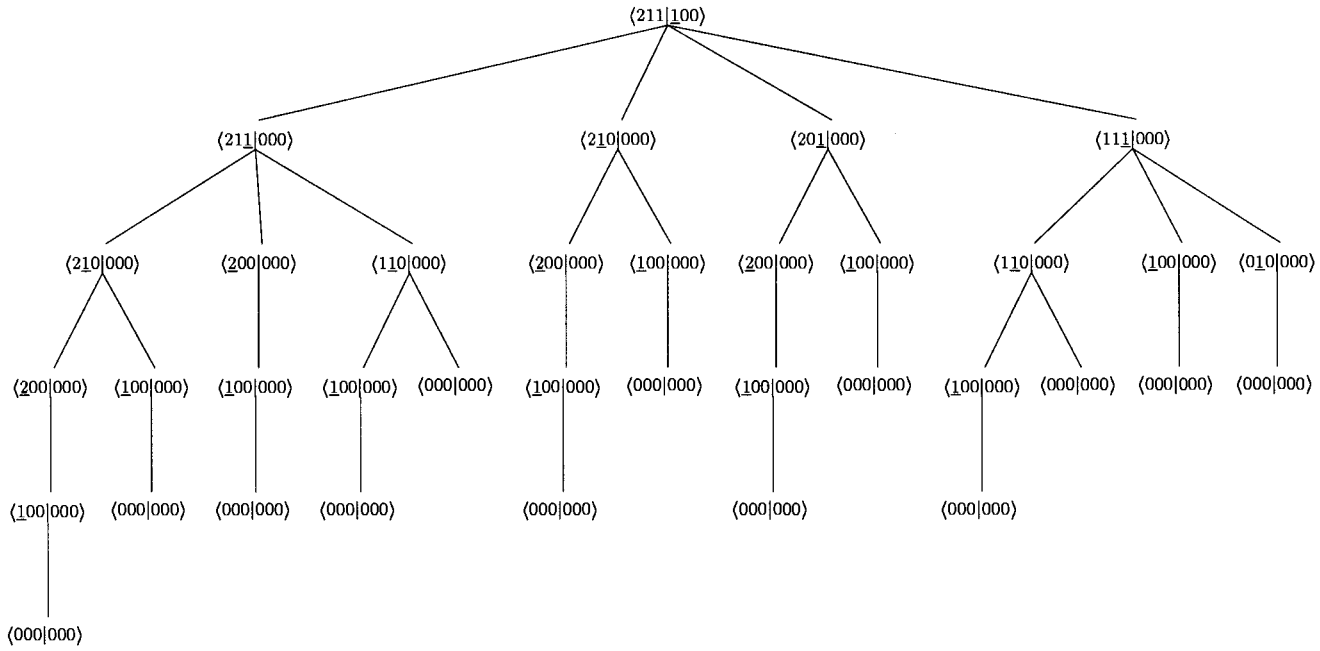

Figure 10. Recurrence tree for the overlap integral ⟨211|100⟩ of a three-dimensional harmonic oscillator. Recurrence relations are applied to the underlined vibrations.

from the more distant $^1B_{1g}$ state, are so low that these lines do not show up in the calculated spectra. Owing to symmetry, single quantum transitions of ν_{16a} (a_u) and ν_{16b} (b_{3u}) are forbidden. These vibrations are observed as hot bands; the spectrum calculated at 300 K gives the correct position and intensity of these lines. In addition, the overtone $16b_0^2$, whose intensity is due to the much smaller frequency of this mode in the excited state, is calculated in good agreement with the experimental spectrum.

6. Conclusion

In agreement with experimental spectra, the results presented for the benzene and pyrazine spectra show clearly that hot bands are an essential feature in room temperature electronic spectra of benzene derivatives. Not only do they determine the overall appearance of the spectra, they also provide characteristic details for their assignment and their analysis in terms of ground- and excited-state potential energy surfaces and detailed shapes of the normal coordinates.

The program HOTFCHT based on the adiabatic and harmonic approximations is well-suited to reproduce all these details in good agreemant with experimental data. Anharmonicity effects like the double-minimum potential due to S_1-S_2 interaction in pyrazine can be taken into account by expanding the eigenstates in terms of harmonic oscillator states.

Work in progress on aromatics as well as hot reaction intermediates will further demonstrate the importance of high-temperature calculations of the vibrational fine structure of electronic transitions in identifying and assigning spectral lines. The ultimate goal of this work is a complete description of photophysical properties including temperature effects.

Acknowledgment. Financial support by DFG and Fonds der Chemischen Industrie as well as computing time provided by the HLRZ Jülich is gratefully acknowledged. Thanks are due to Prof. K. Gustav, Jena, for helpful discussions and a fruitful collaboration in early stages of this work and to Prof. A. Warshel for providing unpublished material.

Appendix

Application of the recurrence relations eqs 11 and 12 to evaluate the overlap integral $\langle\vec{v}'|\vec{v}\rangle$ is schematically illustrated in Figure 10 for a typical integral $\langle 211|100\rangle$ of a three-dimensional oscillator. In the first step the smallest nonzero element of the initial state $\vec{v}$ is chosen as $v_\eta + 1$ in eq 11. In order to evaluate $\langle\vec{v}|v_1, ..., v_{\eta+1}, ..., v_N\rangle$, the integrals $\langle v'_1,...,v'_{\xi-1},...,v'_N|v_1,...,v_\eta,...,v_N\rangle$ and $\langle\vec{v}'|v_1, ..., v_{\zeta-1}, ..., v_N\rangle$, where ξ and ζ run over all N normal modes with nonzero quantum numbers v'_ξ and v_ζ, respectively, as well as the integral $\langle\vec{v}'|v_1, ..., v_\eta, ..., v_N\rangle$ are required and have to be evaluated in the same way by choosing an appropriate η. If only integrals of the type $\langle\vec{v}'|\vec{0}\rangle$ are left, the smallest nonzero quantum number of the final state $\vec{v}'$ is chosen as $v'_\xi + 1$ in eq 12. This procedure is repeated until the integral $\langle\vec{0}'|\vec{0}\rangle$ is reached, which is computed from eq 8.

A brute-force application of this recurrence scheme is highly ineffective due to repeated calculation of integrals (e.g., for the integral in Figure 10 $\langle 200|000\rangle$ would be calculated four times), but this method could be improved in several ways: (i) by storing all calculated Franck−Condon integrals, for instance in a binary tree as suggested by Gruner et al.[32] (conventional method), (ii) by storing some of the calculated Franck−Condon integrals, for instance those of the type $\langle\vec{v}'|\vec{0}\rangle$ (semidirect method), (iii) by conducting the recurrence in such a way through the tree that repeated calculation of the same integrals is more or less strictly avoided (direct method), or, finally, (iv) by calculating the integrals iteratively beginning with $\langle\vec{0}'|\vec{0}\rangle$ and ending at $\langle\vec{v}'|\vec{v}\rangle$ (iterative direct method).

As with increasing temperature the number of overlap integrals becomes exceedingly large, the conventional method is only of limited value; test calculations of the benzene spectrum at 300 K show that the binary tree quickly consumes a few gigabytes of main storage. The semidirect method might be a good compromise for workstation computers, while the direct method uses less than 10 MB core memory for the benzene case and is therefore well-suited even for personal computers. In our current implementation of the recurrent direct method, the number of multiple calculation of integrals is reduced but not completely zero. We therefore expect a significant speedup for an iterative direct scheme.

References and Notes

(1) Klessinger, M.; Michl, J. *Excited States and Photochemistry of Organic Molecules*; VCH: New York, 1995.

(2) Heller, E. J. *Acc. Chem. Res.* **1981**, *14* (12), 368. Luzhkov, V.; Warshel, A. *J. Am. Chem. Soc.* **1991**, *113*, 4491. Schinke, R.; Huber, J. R. In *Femtosecond Chemistry*; Manz, J., Wöste, L., Eds.; VCH: Weinheim, 1995; Vol. 1, p 299.

(3) Woywod, C.; Domcke, W.; Sobolewski, A. L.; Werner, H.-J. *J. Chem. Phys.* **1994**, *100* (2), 1400.

(4) Franck, J. *Trans. Faraday Soc.* **1925**, *21*, 536. Condon, E. U. *Phys. Rev.* **1926**, *28*, 1182. Condon, E. U. *Phys. Rev.* **1928**, *32*, 858.

(5) Sharp, T. E.; Rosenstock, H. M. *J. Chem. Phys.* **1964**, *41*, 3453.

(6) Doktorov, E. V.; Malkin, I. A.; Man'ko, V. I. *J. Mol. Spectrosc.* **1975**, *56*, 1.

(7) Doktorov, E. V.; Malkin, I. A.; Man'ko, V. I. *J. Mol. Spectrosc.* **1977**, *64*, 302.

(8) Faulkner, T. R.; Richardson, F. S. *J. Chem. Phys.* **1979**, *70*, 1201.

(9) Kupka, H.; Cribb, P. H. *J. Chem. Phys.* **1986**, *85*, 1303. Chen, K.; Pei, C. *Chem. Phys. Lett.* **1990**, *165*, 523.

(10) Warshel, A.; Karplus, M. Unpublished.

(11) Baranov, V. I.; Zelent'sov, D. Y. *J. Mol. Struct.* **1992**, *272*, 283.

(12) Warshel, A.; Karplus, M. *J. Am. Chem. Soc.* **1972**, *94*, 5612.

(13) del Bene, J.; Jaffé, H. H. *J. Chem. Phys.* **1968**, *48*, 1807.

(14) Herzberg, G.; Teller, E. *Z. Phys. Chem.* **1933**, *b21*, 410.

(15) Fischer, G. *Vibronic Coupling*; Academic Press Inc.: London, 1984.

(16) Buma, W. J.; Zerbetto, F. *J. Chem. Phys.* **1995**, *103*, 10492.

(17) Warshel, A.; Dauber, P. *J. Chem. Phys.* **1977**, *66*, 5477. Gustav, K.; Storch, M. *Monatsh. Chem.* **1986**, *117*, 1007. Gustav, K.; Storch, M.; Jung, Ch. *Acta Phys. Pol.* **1989**, *A76*, 883. Gustav, K.; Storch, M. *Int. J. Quantum Chem.* **1990**, *38*, 25.

(18) Orlandi, G.; Palmieri, P.; Tarroni, R.; Zerbetto, F.; Zgierski, M. Z. *J. Chem. Phys.* **1994**, *100*, 2458.

(19) Zerbetto, F.; Zgierski, M. Z. *J. Chem. Phys.* **1993**, *98*, 4822.

(20) Negri, F.; Zgierski, M. Z. *J. Chem. Phys.* **1995**, *102*, 5165.

(21) Stein, S. E.; Rabinovitch, B. S. *J. Chem. Phys.* **1973**, *58*, 2438.

(22) Kemper, M. J. H.; van Dijk, J. M. F.; Buck, H. M. *Chem. Phys. Lett.* **1978**, *53*, 121.

(23) Berger, R.; Klessinger, M. *J. Comput. Chem.* **1997**, *18*, 1312.

(24) For a preliminary version of the HOTFCHT program, contact the authors.

(25) Herzberg, G. *Spectra of Diatomic Molecules*, *Molecular Spectra and Molecular Structure*, 2nd ed.; van Nostrand Reinhold Company: Cincinnati, OH, 1950.

(26) Small, G. J. *J. Chem. Phys.* **1971**, *54*, 3300. Hohlneicher, G.; Wolf, J. *Ber. Bunsen-Ges. Phys. Chem.* **1995**, *99*, 366.

(27) Duschinsky, F. *Acta Physicochim. URSS* **1937**, *7*, 551.

(28) Pickett, H. M.; Strauss, H. L. *J. Am. Chem. Soc.* **1970**, *92*, 7281.

(29) Lucas, N. J. D. *J. Phys. B* **1973**, *6*, 155.

(30) Duch, W. *J. Phys.* **1983**, *16A*, 4233.

(31) Radle, W. F.; Beck, C. A. *J. Chem. Phys.* **1940**, *7*, 507.

(32) Gruner, D.; Brumer, P. *Chem. Phys. Lett.* **1987**, *138*, 310.

(33) Dunning, T. H.; Hay, P. J. In *Modern Theoretical Chemistry*; Schaefer, H. F., III, Ed.; Plenum: New York, 1976; pp 1−28.

(34) Frisch, M. J.; Trucks, G. W.; Schlegel, H. B.; Gill, P. M. W.; Johnson, B. G.; Robb, M. A.; Cheeseman, J. R.; Keith, T.; Petersson, G. A.; Montgomery, J. A.; Raghavachari, K.; Al-Laham, M. A.; Zakrzewski, V. G.; Ortiz, J. V.; Foresman, J. B.; Cioslowski, J.; Stefanov, B. B.; Nanayakkara, A.; Challacombe, M.; Peng, C. Y.; Ayala, P. Y.; Chen, W.; Wong, M. W.; Andres, J. L.; Replogle, E. S.; Gomperts, R.; Martin, R. L.; Fox, D. J.; Binkley, J. S.; Defrees, D. J.; Baker, J.; Stewart, J. P.; Head-

Gordon, M.; Gonzalez, C.; Pople, J. A. *Gaussian 94*, Gaussian Inc.: Pittsburgh, PA, 1995.

(35) Schmidt, M. W.; Baldridge, K. K.; Boatz, J. A.; Elbert, S. T.; Gordon, M. S.; Jensen, J. H.; Koseki, S.; Matsunaga, N.; Nguyen, K. A.; Su, S. J.; Winduns, T. L.; Dupius, M.; Montgomery, J. A. *J. Comput. Chem.* **1993**, *14*, 1347.

(36) MOLPRO is a suite of ab initio programs written by H.-J. Werner and P. J. Knowles, with contributions by J. Almöf, R. D. Amos, S. T. Elbert, W. Meyer, E.-A. Reinsch, R. M. Pitzer, A. J. Stone, and P. R. Taylor.

(37) Werner, H.-J.; Knowles, P. J. *J. Chem. Phys.* **1988**, *89*, 5803. Knowles, P. J.; Werner, H.-J. *Chem. Phys. Lett.* **1988**, *145*, 514.

(38) Turkevich, A.; Fred, M. *Rev. Mod. Phys.* **1942**, *14*, 246.

(39) Callomon, J. H.; Dunn, T. M.; Mills, I. M. *Trans. R. Soc. London* **1966**, *259*, 499.

(40) Knight, A. E. W.; Parmenter, C. S.; Schuyler, M. W. *J. Am. Chem. Soc.* **1975**, *97*, 1993.

(41) Knight, A. E. W.; Parmenter, C. S.; Schuyler, M. W. *J. Am. Chem. Soc.* **1975**, *97*, 2005.

(42) Atkinson, G. H.; Parmenter, C. S. *J. Mol. Spectrosc.* **1978**, *73*, 20.

(43) Fischer, G.; Jakobson, S. *Mol. Phys.* **1979**, *38*, 299.

(44) Stephenson, T. A.; Radloff, P. L.; Rice, S. A. *J. Chem. Phys.* **1984**, *81*, 1060.

(45) Page, R. H.; Shen, Y. R.; Lee, Y. T. *J. Chem. Phys.* **1988**, *88*, 5362.

(46) Craig, D. P. *J. Chem. Soc.* **1940**, 2146.

(47) Albrecht, A. C. *J. Chem. Phys.* **1960**, *33*, 169. Ziegler, L.; Albrecht, A. C. *J. Chem. Phys.* **1974**, *60*, 3558. Metz, F.; Robey, M. J.; Schlag, E. W.; Dörr, F. *Chem. Phys. Lett.* **1977**, *51*, 8. Fischer, G.; Reimers, J. R.; Ross, I. G. *Chem. Phys.* **1981**, *62*, 187. Orlandi, G.; Zerbetto, F. *Chem. Phys.* **1986**, *108*, 197.

(48) O'Connor, D.; Sumatini, M.; Takagi, Y.; Nakashima, N.; Udagawa, Y.; Yoshihira, K. *J. Phys. Chem.* **1983**, *87*, 4848.

(49) Robey, M. J.; Schlag, E. W. *J. Chem. Phys.* **1977**, *67*, 2775. Pulay, P.; Fogarasi, G.; Boggs, J. E. *J. Chem. Phys.* **1981**, *74*, 3999. Krogh-Jespersen, K.; Rava, R. P.; Goodman, L. *J. Phys. Chem.* **1984**, *88*, 5503. Ozkabak, A. G.; Goodman, L.; Thakur, S. N.; Krogh-Jespersen, K. *J. Chem. Phys.* **1985**, *83*, 6047. Pulay, P. *J. Chem. Phys.* **1986**, *85*, 1703. Ozkabak, A. G.; Goodman, L. *J. Chem. Phys.* **1987**, *87*, 2564. Kato, S. *J. Chem. Phys.* **1988**, *88*, 3045. Maslen, P. E.; Handy, N. C.; Amos, R. D.; Jayatilaka, D. *J. Chem. Phys.* **1992**, *97*, 4233. Wyatt, R. E.; Christophe, I. *J. Chem. Phys.* **1993**, *98*, 6758.

(50) Swiderek, P.; Hohlneicher, G.; Maluendes, S. A.; Dupius, M. *J. Chem. Phys.* **1993**, *98*, 974.

(51) Shaik, S.; Zilberg, S.; Haas, Y. *Acc. Chem. Res.* **1996**, *29*, 211. Shaik, S.; Shurki, A.; Danovich, D.; Hilberty, P. C. *J. Am. Chem. Soc.* **1996**, *118*, 666.

(52) Ozkabak, A. G.; Goodman, L.; Wiberg, K. B. *J. Chem. Phys.* **1990**, *92*, 4115.

(53) Udagawa, Y.; Ito, M. *Chem. Phys.* **1980**, *46*, 237.

(54) McDonald, D. B.; Rice, S. A. *J. Chem. Phys.* **1981**, *74*(9), 4893.

(55) Thakur, S. N.; Innes, K. K. *J. Mol. Spectrosc.* **1974**, *52*, 130.

(56) Zalewski, E. F.; McClure, D. S.; Narva, D. L. *Chem. Phys.* **1974**, *61* (7), 2964.

(57) Esherick, P.; Zinsli, P.; El-Sayed, M. A. *Chem. Phys.* **1975**, *10*, 415. Knoth, I.; Neusser, H. J.; Schlag, E. W. *Z. Naturforsch.* **1978**, *43a*, 979. Venuti, E.; Marconi, G. *Chem. Phys.* **1988**, *125*, 1.

(58) Hong, H.-K.; Jakobsen, C. W. *J. Chem. Phys.* **1978**, *68*, 1170. Suzuka, I.; Udagawa, Y.; Ito, M. *Chem. Phys. Lett.* **1979**, *64*, 333. Stock, G.; Woywod, C.; Domcke, W.; Swinney, T.; Hudson, B. S. *J. Chem. Phys.* **1995**, *103* (16), 6851.

(59) Yamazaki, I.; Fujita, M.; Baba, H. *Chem. Phys.* **1981**, *57*, 431. Yamazaki, I.; Murao, T.; Yoshihara, K. *Chem. Phys. Lett.* **1982**, *87* (4), 384. Sekiguchi, O.; Ohta, N.; Baba, H. *Bull. Chem. Soc. Jpn.* **1984**, *57*, 3591.

(60) Schneider, R.; Domcke, W. *Chem. Phys. Lett.* **1988**, *150*, 235.

(61) Baranov, V. I.; Ten, G. N.; Gribov, L. A. *J. Mol. Struct.* **1986**, *137*, 91.

(62) Baranov, V. I.; Gribov, L. A.; Djenjer, O. V.; Zelent'sov, D. Yu. *J. Mol. Struct.* **1997**, *407*, 209.

(63) Seidner, L.; Stock, G.; Sobolewski, A. L.; Domcke, W. *J. Chem. Phys.* **1992**, *96* (7), 5298.

(64) Martin, J. M. L.; van Alsenoy, C. *J. Phys. Chem.* **1996**, *100* (17), 6973.

(65) Cradock, S.; Liescheski, P. B.; Rankin, D. W. H.; Robertson, H. E. *J. Am. Chem. Soc.* **1988**, *110* (9), 2758.

(66) Bormans, B. J. M.; de With, G. *J. Mol. Struct.* **1977**, *42*, 121.

(67) Lord, R. C.; Marston, A. L.; Miller, F. A. *Spectrochim. Acta* **1957**, *9*, 113.

(68) Innes, K. K.; Ross, I. G.; Moomaw, W. R. *J. Mol. Spectrosc.* **1988**, *132*, 492.

(69) Kearly, G. J.; Tomkinson, J.; Navarro, A.; Gonzalez, López Gómez, J. J.; Fernández Gómez, M. *Chem. Phys.* **1997**, *216*, 323.

(70) Azumi, T.; Matsuzaki, K. *Photochem. Photobiol.* **1977**, *25*, 315.

(71) Kanamaru, N.; Lim, E. C. *Chem. Phys. Lett.* **1975**, *35* (3), 303.

(72) Narva, D. L.; McClure, D. S. *Chem. Phys.* **1975**, *11*, 151. Chappell, D. J.; Ross, I. G. *Chem. Phys. Lett.* **1976**, *43*, 440. Gregory, A. R.; Henneker, W. H.; Siebrand, W.; Zgierski, M. Z. *J. Chem. Phys.* **1978**, *65* (7), 1884. Udagawa, Y.; Ito, M.; Suzuka, I.; Siebrand, W.; Zgierski, M. Z. *Chem. Phys. Lett.* **1979**, *68*, 258.

(73) Tsuboi, M.; Hirakawa, A. Y. *J. Raman Spectrosc.* **1976**, *5*, 75. Lee, S.-Y. *J. Chem. Phys.* **1990**, *92* (11), 6376.

(74) Wassam, W. A., Jr.; Lim, E. C. *Chem. Phys.* **1979**, *42*, 149. Brickmann, J. *Ber. Bunsen-Ges. Phys. Chem.* **1979**, *83*, 70. Gustav, K.; Colditz, R. *Int. J. Quantum Chem.* **1982**, *22*, 31.

(75) Heider, N.; Fischer, S. F. *Chem. Phys.* **1984**, *88*, 209.

(76) Schneider, R.; Domcke, W. *Chem. Phys. Lett.* **1989**, *159* (1), 61. Schneider, R.; Domcke, W.; Köppel, H. *J. Chem. Phys.* **1990**, *92* (2), 1045. Stock, G.; Domcke, W. *J. Chem. Phys.* **1990**, *93* (8), 5496. Domcke, W.; Sobolewski, A. L.; Woywod, C. *Chem. Phys. Lett.* **1993**, *203*, 220. Stock, G.; Domcke, W. *J. Phys. Chem.* **1993**, *97* (48), 12466.

(77) Rauhut, G.; Pulay, P. *J. Phys. Chem.* **1995**, *99*, 3093.

(78) Udagawa, Y.; Ito, M. *Chem. Phys.* **1978**, *60* (1), 25.

(79) Neusser, H. J.; Schlag, E. W. *Angew. Chem.* **1992**, *104*, 269.

(80) Stephenson, T. A.; Rice, S. A. *J. Chem. Phys.* **1984**, *81*, 1073.

(81) Yamazaki, I.; Murao, T.; Yamanaka, T.; Yoshihara, K. *Faraday Discuss. Chem. Soc.* **1983**, *75*, 395.